Journal of Alloys and Compounds 509 (2011) 2401–2406

Contents lists available at ScienceDirect

Journal of Alloys and Compounds

journal homepage: www.elsevier.com/locate/jallcom

Structural analysis and properties of thermally stable $Ba_8Mg(Nb_{6-x}Sb_x)O_{24}$ microwave ceramics

M.K. Suresh[a], Annamma John[a,1], J.K. Thomas[a], P.R.S. Wariar[b], Sam Solomon[a,*]

[a] Department of Physics, Mar Ivanios College, Thiruvananthapuram 695 015, Kerala, India
[b] Department of Physics, University College, Thiruvananthapuram 695 034, Kerala, India

ARTICLE INFO

Article history:
Received 22 June 2010
Received in revised form 3 November 2010
Accepted 4 November 2010
Available online 13 November 2010

Keywords:
Ceramics
Sintering
Dielectric
Optical spectroscopy

ABSTRACT

$Ba_8Mg(Nb_{6-x}Sb_x)O_{24}$ (x = 0, 0.3, 0.6, 0.9, 1.2, 1.5, 1.8 and 2.4) ceramics were prepared through conventional solid-state route. The materials were calcined at 1200 °C and sintered at the optimized temperature of 1375 °C. The structure of the system was analyzed by X-ray diffraction, Fourier transform infrared and Raman spectroscopic methods. The theoretical and experimental densities were calculated. The dielectric constant (ε_r), temperature coefficient of resonant frequency (τ_f) and the unloaded quality factor (Q_u) were measured in the microwave frequency region using cavity resonator method. The τ_f values of the samples reduced considerably with the increase in Sb concentration. The dielectric responses were studied in the frequency range 50 Hz to 5 MHz also. The microstructure of the sintered pellets was analyzed using scanning electron microscopy. The materials have intense emission lines in the visible region. The compositions have good microwave dielectric properties and photoluminescence and hence are suitable for dielectric resonator and ceramic laser applications.

1. Introduction

Resonators are important components in microwave and radio frequency communication equipments in connection with filters, low noise oscillators, triplexers, antennas and other circuits. Dielectric resonators (DRs) provide significant advantages in terms of compactness, light mass, temperature stability and relatively low cost of production. DRs are frequently employed in wireless and mobile communications should have relatively high quality factor (Q_u) for selectivity, high dielectric constant (ε_r) for miniaturization and low temperature coefficient of resonant frequency (τ_f) for good frequency stability [1–3]. Owing to the flexibility of the compounds with complex perovskite type structure having general formula $A(B'B'')O_3$ which allows extensive modifications in both A and B sites, have been designed and widely used in industrial applications. The compounds with complex perovskite type structure such as $Ba(Mg_{1/3}Ta_{2/3})O_3$ and $Ba(Zn_{1/3}Ta_{2/3})O_3$ are widely used in the area of wireless communication systems and many researchers are working on such compounds [4–10]. Molodesky and Davies [11] have reported the microwave dielectric properties of 1:1 or 1:2 cation ordering perovskites such as $Ba(Y_{1/2}Nb_{1/2})O_3$ and $Ba(Co_{1/3}Nb_{2/3})O_3$. Extensive work is going on tantalate and niobate complex perovskites due to their high polarizability and wide compositional tuning opportunities offered by the substitutional flexibility of mixed B-site perovskites. Abakumov [12] have analyzed the crystal structure of $Ba_8Ta_6NiO_{24}$ ceramic and found that it has hexagonal perovskite structure with a space group of $P6_3cm$ in which Ta and Ni cations has the symmetric sixfold oxygen co-ordinates in the TaO_6 and NiO_6 octahedra. Moussa et al. [13] synthesized $Ba_8ZnTa_6O_{24}$ and its crystallographic properties were characterized using Rietveld refinement. Davies et al. [14] prepared densified single phase samples of $Ba_8ZnTa_6O_{24}$ and found to be isostructural with $Ba_8NiTa_6O_{24}$, a structure based on 8H $(cchc)_2$ close-packed arrangement of BaO_3 stacking sequence and the lattice parameters, a = 10.0825 Å, c = 19.0587 Å. It is reported that $Ba_8ZnTa_6O_{24}$ is a hexagonal perovskite and which is found to be a stable secondary phase, formed as a result of the loss of ZnO from $Ba(Zn_{1/3}Ta_{2/3})O_3$ microwave dielectrics during the high temperature calcinations and sintering treatments [15]. Barwick et al. [16] reported that $Ba_8ZnNb_6O_{24}$ is a secondary phase of $Ba(Zn_{1/3}Nb_{2/3})O_3$, which is formed to compensate for the Zn vacancies resulting from the lost material during processing. This is analogous to $Ba_8ZnTa_6O_{24}$, the impurity phase found in $Ba(Zn_{1/3}Ta_{2/3})O_3$ ceramics. The $Ba_8ZnNb_6O_{24}$ is a perovskite-type structure, with regular stacking faults, giving recurrent planes of face-sharing (as opposed to corner-sharing) oxygen octahedra. It is reported that $Ba_8ZnNb_6O_{24}$ exhibits hexagonal structure with space group $P6_3cm$ and lattice parameters a = 10.0643 Å and c = 19.0060 Å [17,18]. Kawaguchi et al. [19]

* Corresponding author at: Department of Physics, St. John's College, Anchal, Kollam District, 691306 Kerala, India. Tel.: +91 9847314237; fax: +91 471 2532445.
E-mail address: samdmrl@yahoo.com (S. Solomon).
[1] Department of Physics, St. John's College, Anchal, Kollam District, 691306 Kerala, India.

0925-8388/$ – see front matter © 2010 Elsevier B.V. All rights reserved.
doi:10.1016/j.jallcom.2010.11.029

investigated the effect of M (M = Zn and Mg) substitution for Ni on the microwave dielectric properties and crystal structure of $Ba_8Ta_6(Ni_{1-x}M_x)O_{24}$ ($x = 0$–1) ceramics. Photoluminescence (PL) is the spontaneous emission of light from a material under optical excitation. PL spectrum provides the transition energies, which can be used to determine electronic energy levels and the intensity, which provides the information on the quality of the surfaces and interfaces and gives a measure of relative rates of radiative and non-radiative recombination [20]. Inorganic luminescent crystalline materials are increasingly important in the development of smaller, faster and more efficient electronic and optoelectronic devices [21–23].

In this paper we report the synthesis, characterization, IR, Raman, dielectric and photoluminesent studies of $Ba_8Mg(Nb_{6-x}Sb_x)O_{24}$ ($x = 0$, 0.3, 0.6, 0.9, 1.2, 1.5, 1.8 and 2.4) ceramics, for the first time.

2. Experimental method

$Ba_8Mg(Nb_{6-x}Sb_x)O_{24}$ ($x = 0$, 0.3, 0.6, 0.9, 1.2, 1.5, 1.8 and 2.4) ceramics are prepared through the conventional solid-state route. The high purity (>99%) $BaCO_3$, MgO, Nb_2O_5 and Sb_2O_5 are weighed in stoichiometric ratios and ball milled, using zirconia balls in plastic containers and acetone as wetting medium, for 2 h. The samples are dried and calcined at 1200 °C for 6 h in electrically heated furnace. The calcined powder is again ball milled for 6 h and the slurry is dried and ground well in agate mortar. Polyvinyl alcohol (5 wt%) is added to this powder as binder, again ground well and dried. The powder is then pressed in the form of cylindrical pellets at a pressure of 100 MPa using hydraulic press. The pellets are then sintered at the temperature 1375 °C for 5 h in a controlled heating schedule. The sintered samples are polished well and the densities are calculated by the Archimedes method. Powdered samples are used for X-ray diffraction (Philips Expert Pro) studies using CuKα radiation. The theoretical densities of the samples are calculated using the least-square method. The infrared (IR) spectra of the samples are recorded in the range 400–4000 cm^{-1} on a Perkin Elmer Fourier Transform Infrared (FT-IR) Spectrometer (Spectrum RX1) using KBr pellet method. The Fourier Transform-Raman spectrum is recorded at room temperature in the wave number range 50–850 cm^{-1} using Bruker RFS/100S Spectrometer at a power level of 150 mW and at a resolution of 4 cm^{-1}. The samples are excited with an Nd: YAG laser lasing at 1064 nm and the scattered radiations are detected using Ge detector. The dielectric properties in the microwave frequency range are measured using cavity resonator method by the computer interfaced network analyzer (Agilent 8753 ET). The temperature coefficient of resonant frequency (τ_f) is measured over a range of temperature 30–70 °C with the help of experimental setup attached to the network analyzer. The radio frequency dielectric properties of the samples are studied using an LCR meter (Hioki-3532-50) in the frequency range 50 Hz to 5 MHz by making them in the form of a disc capacitor with the specimen as the dielectric medium with silver electrodes on both sides of the circular disc. Polished samples are thermally etched at 1325 °C for half an hour and used for Scanning Electron Microscope (SEM, JEOL Model 6390 LV). The photoluminescent spectra, at room temperature, are recorded using Perkin Elmer LS55 spectrophotometer.

3. Results and discussion

The X-ray diffraction (XRD) patterns of sintered $Ba_8Mg(Nb_{6-x}Sb_x)O_{24}$ ($x = 0$, 0.9, 1.2, 1.5, 1.8 and 2.4) ceramics are given in Fig. 1. All the peaks can be indexed using the structure of $Ba_8Ta_6NiO_{24}$ ceramics (ICDD file 89-0693), which has a hexagonal perovskite structure (space group $P6_3cm$) based on an 8H $(cchc)_2$ close packed arrangement of BaO_3 layers, with $Z = 3$ [12–14]. Fig. 2 shows the magnified XRD patterns of $Ba_8MgNb_6O_{24}$ ($x = 0$) and $Ba_8Mg(Nb_{3.6}Sb_{2.4})O_{24}$ ($x = 2.4$) and it is clear that there is no change in the structure with the increase of Sb concentration. The lattice parameters and cell volume of the samples are calculated using the least square method and are given in Table 1. The theoretical and experimental densities are also given in the table. The theoretical density increases with the increase in Sb concentration due to the higher atomic weight of Sb atom. The experimental densities of the pellets are above 90% of the theoretical values and decreasing with the increase in the concentration of Sb. The decrease in experimental density for the higher concentrations of Sb is due to the decrease in sinterability. This may be due to the difference in ionic radii between Nb^{5+} (0.64 Å) and Sb^{5+} (0.6 Å) [24]. Fig. 3 shows the variation of experimental density with temperature.

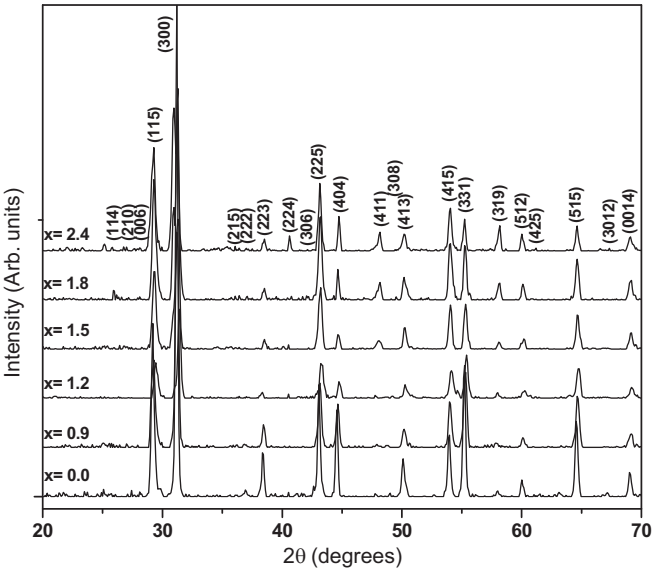

Fig. 1. XRD patterns of $Ba_8Mg(Nb_{6-x}Sb_x)O_{24}$ ceramics.

The Raman spectra of the two end samples, $Ba_8MgNb_6O_{24}$ and $Ba_8Mg(Nb_{3.6}Sb_{2.4})O_{24}$, are recorded over the range 50–900 cm^{-1}. The spectrum of $Ba_8MgNb_6O_{24}$ is shown in Fig. 4. The spectrum obtained for $Ba_8Mg(Nb_{3.6}Sb_{2.4})O_{24}$ is highly noisy and therefore that figure is not included. However, the intense peaks are easily identifiable and are found to be sharper, with very little change in position, than that of the parent sample. The observed Raman bands of $Ba_8MgNb_6O_{24}$, their relative intensities and their band assignments are given in Table 2. The IR spectra of all the eight samples are recorded to monitor the changes to the characteristic bands on replacing the Nb atom with Sb atom in different concentrations. Fig. 5 shows the IR spectra of the samples over the range 4000–400 cm^{-1} and Fig. 6 shows the IR spectra of the end samples over the range 900–400 cm^{-1}.

As reported by Abakumov [12] for $Ba_8Ta_6NiO_{24}$, it is expected that $Ba_8MgNb_6O_{24}$ too have two different pairs of face sharing octahedra. In the first pair, one octahedron is occupied by Nb atoms

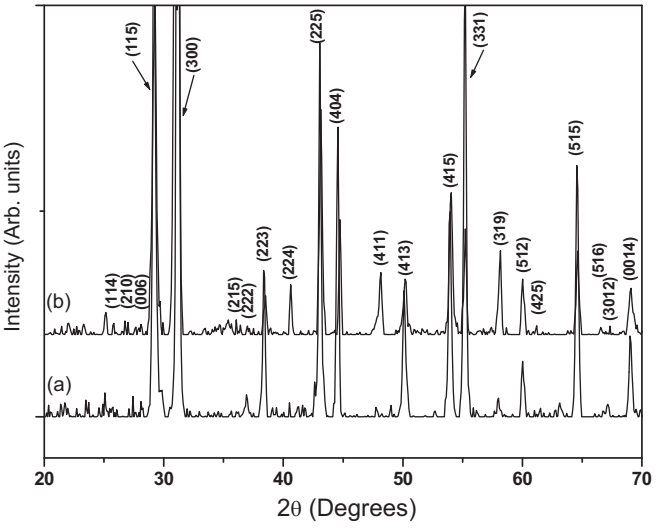

Fig. 2. Magnified XRD patterns of (a) $Ba_8MgNb_6O_{24}$ and (b) $Ba_8Mg(Nb_{3.6}Sb_{2.4})O_{24}$ ceramics.

Table 1
The lattice parameters, unit cell volume and density of $Ba_8Mg(Nb_{6-x}Sb_x)O_{24}$ (x = 0, 0.9, 1.2, 1.5, 1.8 and 2.4) ceramics.

x	Lattice parameters		Cell volume (Å^3)	Theoretical density (g/cm^3)	Experimental density (g/cm^3)
	a (Å)	c (Å)			
0	9.9939	19.3772	1676.0378	6.1707	6.0689
0.9	9.9821	19.3546	1670.1048	6.2705	6.1783
1.2	9.9598	19.3260	1660.2002	6.3340	6.1242
1.5	9.9735	19.3138	1663.7093	6.3467	6.0828
1.8	9.9882	19.2675	1664.6328	6.3693	6.0119
2.4	10.0057	19.1782	1662.7102	6.4289	5.9392

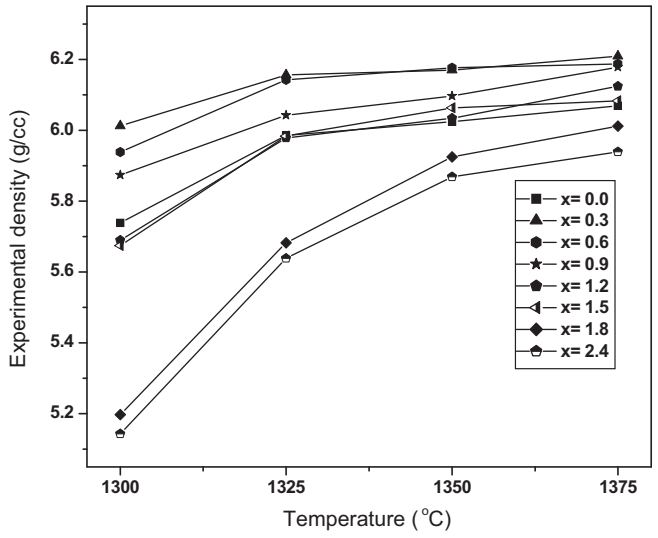

Fig. 3. Variation of experimental density with temperature.

Table 2
Raman spectral data, their relative intensities and band assignments of $Ba_8MgNb_6O_{24}$ ceramic.

$Ba_8MgNb_6O_{24}$	Band assignments
848 m	
	υ_1A_{1g}
779 vs	
543 wbr	υ_3F_{1u}
474 vw	
	υ_2E_g
440 m	
385 m	
	υ_5F_{2g}
310 vs	
263 vw	
	υ_6F_{2u}
242 w	
160 m	
115 s	Lattice modes
105 m	
85 w	

Relative intensities: v, very; s, strong; m, medium; w, weak; br, broad.

whereas the other one is empty. In the second pair, one of the octahedra is occupied Nb and a cation vacancy and its neighbor is occupied by Mg, Nb or a vacancy. This leads to the presence of distorted as well as undistorted close to ideal octahedra in the compound. The Raman active modes of NbO_6 octahedron namely the υ_1A_{1g} mode, the υ_2E_g mode and υ_5F_{2g} mode are observed as intense bands in the Raman spectrum of $Ba_8MgNb_6O_{24}$. In $Ba_8MgNb_6O_{24}$, the symmetric stretching mode of vibration of the octahedron υ_1A_{1g} is observed as a doublet with components at 848 and 779 cm^{-1} [25,26]. The asymmetric stretching mode υ_2E_g also shows a doublet structure with a medium intense component at 440 cm^{-1} and a very weak counterpart at 474 cm^{-1}. The symmetric bending mode of vibration of the octahedron υ_5F_{2g} contributes the sharp intense bands at 385 and 310 cm^{-1} [27–29]. The splitting exhibited by all the characteristic bands indicates the presence of octahedra with different atoms or a vacancy at the centre. It can also be due to the presence of distorted and undistorted octahedra in the compound.

In the IR spectrum of $Ba_8MgNb_6O_{24}$, a very strong and broad absorption band ranging from 500 to 750 cm^{-1} is observed with

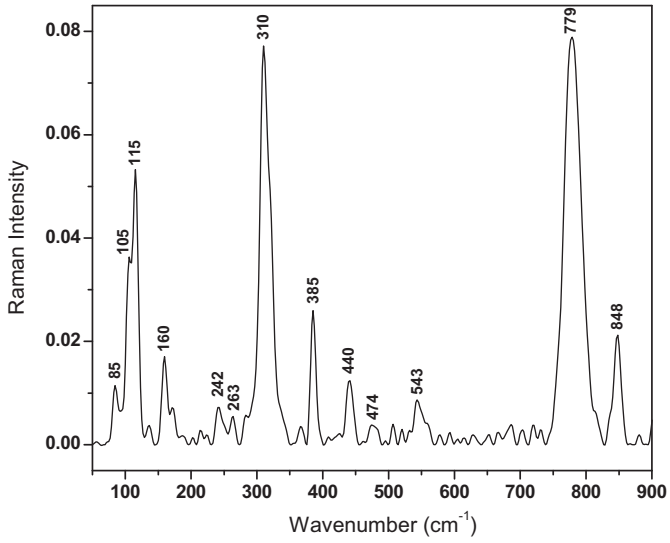

Fig. 4. Raman spectrum of $Ba_8MgNb_6O_{24}$ ceramic.

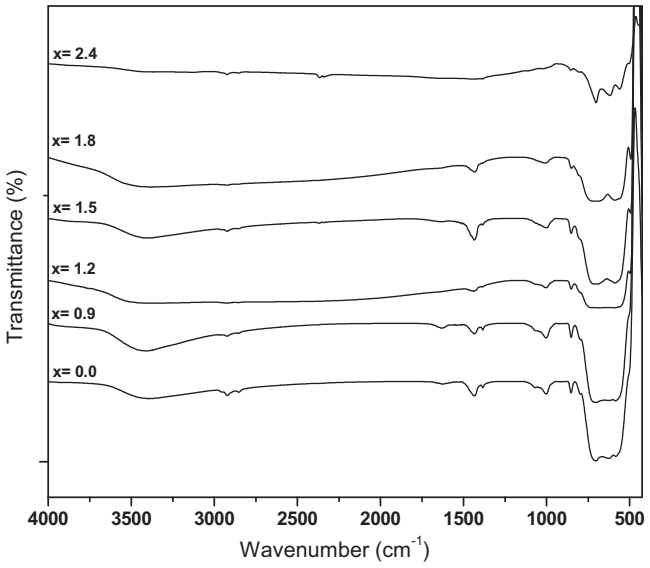

Fig. 5. FT-IR spectra of $Ba_8Mg(Nb_{6-x}Sb_x)O_{24}$ ceramics.

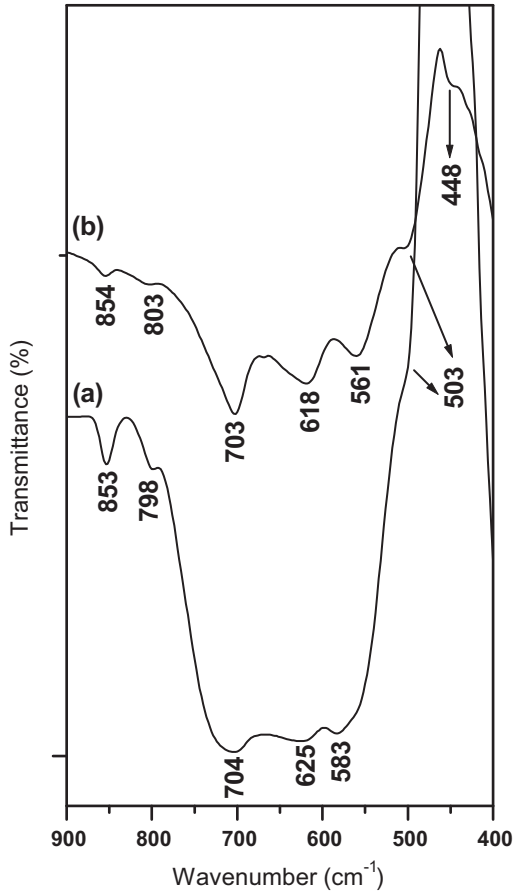

Fig. 6. FT-IR spectra of (a) $Ba_8MgNb_6O_{24}$ and (b) $Ba_8Mg(Nb_{3.6}Sb_{2.4})O_{24}$ ceramics.

distinguishable peaks at 704, 625 and 583 cm^{-1} and a shoulder at 503 cm^{-1}. This broad band with quadruplet structure is due to the υ_3F_{1u} mode of vibration of the different types of octahedra present in the compound. In the IR spectrum of $Ba_8Mg(Nb_{3.6}Sb_{2.4})O_{24}$, these peaks have become sharp and distinct with very little change in the wavenumber. Both the Raman and IR spectrum show that the characteristic bands have become sharper on increasing the concentrations of Sb atoms indicating that the system has become more ordered on replacing the Nb atoms with the heavier Sb atoms. Due to the lower site symmetry of the octahedron, this IR active mode has become active in the Raman spectrum and is observed as a weak band at 543 cm^{-1} which also shows some broadening and tendency of splitting. The silent υ_6F_{2u} mode is observed as very weak bands at 263 and 242 cm^{-1} in the Raman spectrum.

The microwave dielectric properties of the ceramics are given in Table 3. The $Q_u \times f$ value is obtained for $Ba_8MgNb_6O_{24}$ is 18,000 GHz, at 4.04 GHz. When the value of x increases from 0.3 to 2.4 in $Ba_8Mg(Nb_{6-x}Sb_x)O_{24}$, the $Q_u \times f$ values are decreased from 22,900 to 10,500 GHz. The dielectric constant of the ceramics is gradually decreased from 35.9 to 20.6 when the value of x increases from 0 to 2.4 and correspondingly, the τ_f values decrease from 66.1 to 1.5 ppm/°C. Kawaguchi et al. [19] reported that $Ba_8MgTa_6O_{24}$ has the dielectric constant of ~27, $Q_u \times f$ of ~81,000 GHz and τ_f of ~18 ppm/°C. For $Ba_8ZnTa_6O_{24}$, the dielectric constant of ~29, $Q_u \times f$ of ~68,000 GHz and τ_f of ~29 ppm/°C was obtained [13]. Ogawa et al. [30] suggested that the Nb substitution for Ta decreases the covalency of the Ta–O bond and hence decreases $Q_u \times f$ value and increases the dielectric constant. They also suggested that the Sb substitution for Nb enhances the covalency of Sb–O bond and hence the $Q_u \times f$ values increase and dielectric constant decreases. Moreover, Guo et al. [31] suggested that the difference in the dielectric

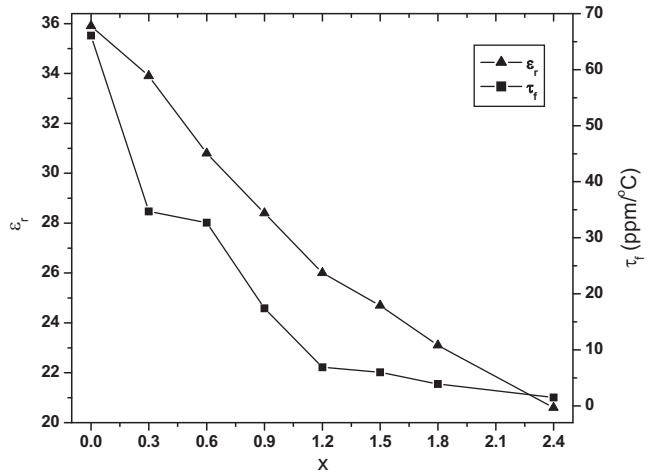

Fig. 7. Variation of dielectric constant (ε_r) and temperature coefficient of resonant frequency (τ_f) with x.

constant between the $Sr(Al_{1/2}Nb_{1/2})O_3$ and $Sr(Al_{1/2}Ta_{1/2})O_3$ ceramics is due to the variations in the bond strength of Nb–O and Ta–O bonds. It may be the reason for the decrease in $Q_u \times f$ value and increase in the dielectric constant of $Ba_8MgNb_6O_{24}$ compared to the above mentioned ceramics in the same family. In our study, the dielectric constant decreases with the increase of Sb concentration and the $Q_u \times f$ values increase firstly then decreases due to the decrease of sinterability. The comparison in the variation of dielectric constant (ε_r) and temperature coefficient of resonant frequency (τ_f) with x is made in Fig. 7.

The dielectric properties of the sintered pellets are studied also in the frequency range 50 Hz to 5 MHz at room temperature. The variation of dielectric constant (ε_r) with frequency (log$f$) is shown in Fig. 8. The observed normal dielectric behavior (i.e., the decrease in the dielectric constant with increasing frequency) is attributed to Maxwell–Wagner interfacial polarization [32]. The decrease in dielectric constant is due to the fact that polarization does not occur instantaneously with the application of the electric field because of inertia. The delay in response towards the electric field leads to decrease in dielectric constant. At low frequencies, all the polarizations contribute. When frequency increases, those with large relaxation time cease respond and results the decrease of dielectric

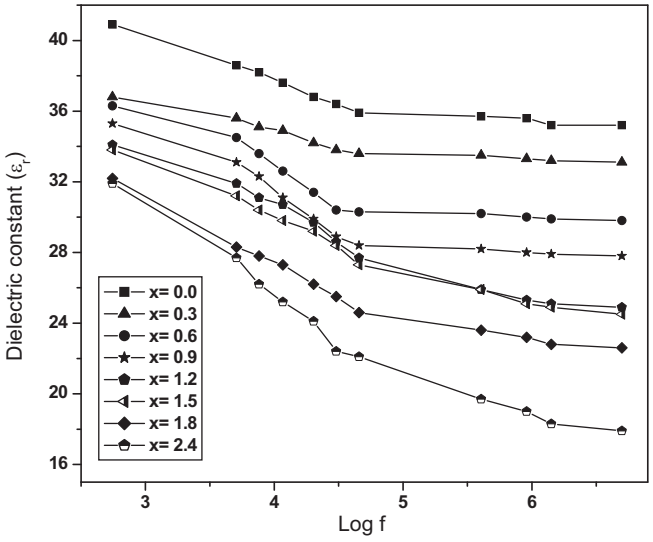

Fig. 8. Variation of dielectric constant (ε_r) with frequency.

Table 3
Microwave dielectric properties of $Ba_8Mg(Nb_{6-x}Sb_x)O_{24}$ ceramics.

x	Dimensions		Resonant frequency f (GHz)	$Q_u \times f$ (GHz)	Dielectric constant (ε_r)	τ_f (ppm/°C)
	Thickness $\times 10^{-3}$ (m)	Diameter $\times 10^{-3}$ (m)				
0	6.34	12.45	4.04	18,000	35.9	+66.1
0.3	6.45	12.49	4.83	22,900	33.9	+34.7
0.6	6.28	12.53	5.10	13,670	30.8	+32.7
0.9	6.66	12.54	4.55	13,070	28.4	+17.4
1.2	6.37	12.63	4.78	12,150	26.0	+6.9
1.5	6.25	12.73	4.90	10,540	24.7	+6.0
1.8	6.36	12.88	5.01	10,780	23.1	+3.9
2.4	6.04	12.97	5.35	10,500	20.6	+1.5

constant [33–35]. The dielectric constant (ε_r) decreases from 35.5 to 18.9 when the value of x increases from 0 to 2.4, at 1 MHz. The variation of loss factor ($\tan\delta$) with frequency is shown in Fig. 9(a) and (b) and it is observed that the loss factor is decreasing with increase in frequency and is in the order of 10^{-3} for the values $x = 0$–0.9 and 10^{-2} for $x = 1.2$–2.4, at 1 MHz. The decrease of loss factor ($\tan\delta$) with the increase of frequency may be described on the basis of Koops phenomenological model [36]. It is observed that the dielectric constant and loss factor decrease with the increase in frequency, for all the compositions.

The SEM micrographs of $Ba_8MgNb_6O_{24}$ ($x = 0$) and $Ba_8Mg(Nb_{3.6}Sb_{2.4})O_{24}$ ($x = 2.4$) ceramics are given in Figs. 10 and 11, respectively. The microstructure of $Ba_8MgNb_6O_{24}$ exhibits the compression of "bar" and "plate-let" shaped grains with minimal porosity. But in the case of $Ba_8Mg(Nb_{3.6}Sb_{2.4})O_{24}$, an abnormal grain growth and a melting nature can be observed. The experimental densities of the samples are decreasing from 98% to 92% of theoretical density with the increase of x from 0 to 2.4, when sintered at 1375 °C for 5 h. These may be the reasons for the reduction of $Q_u \times f$ for the compositions from $x = 1.5$ to 2.4.

The emission spectra are recorded by exciting the samples at the wavelength 400 nm. The photoluminesent spectra of $Ba_8Mg(Nb_{6-x}Sb_x)O_{24}$ ($x = 0$, 0.9, 1.2, 1.8 and 2.4) are recorded between the wavelength 450 and 625 nm and is given in Fig. 12. All the samples show the emission lines at same wavelengths and it indicates that there is no effect with the substitution of Sb atom. A strong emission line is observed at 599 nm due to the transition $^3D_2$–$^3P^0_2$ of Ba atom. The medium emission lines observed at 478 and 529 nm are due to the transitions $^4F_{1.5}$–$^4P^0_{0.5}$ and $^4F_{1.5}$–$^4D^0_{0.5}$, respectively, of Nb atom. Other emission line observed at 532 nm is also due to the transition $^6D_{0.5}$–$^6F^0_{0.5}$ of Nb atom. The samples are very useful for optoelectronic applications such as lasers and optical amplifiers because of their strong emission intensity in the visible region.

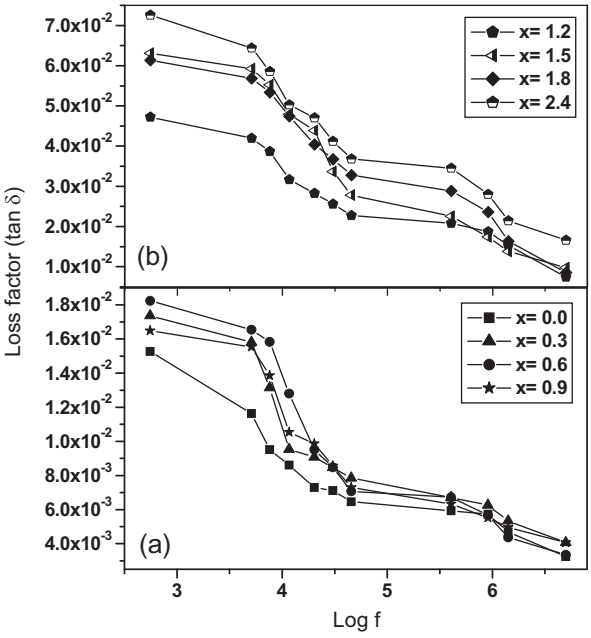

Fig. 9. Variation of loss factor ($\tan\delta$) with frequency.

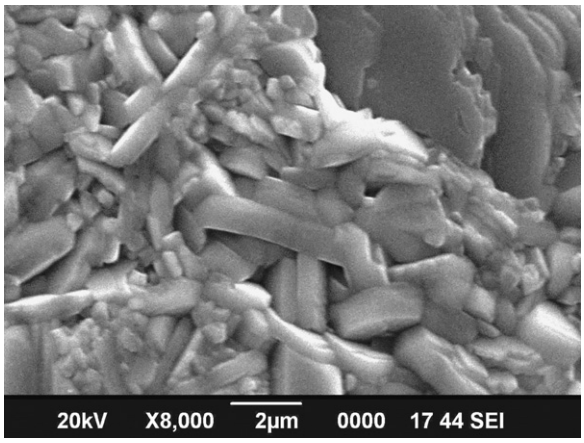

Fig. 10. SEM image of $Ba_8MgNb_6O_{24}$ ceramic.

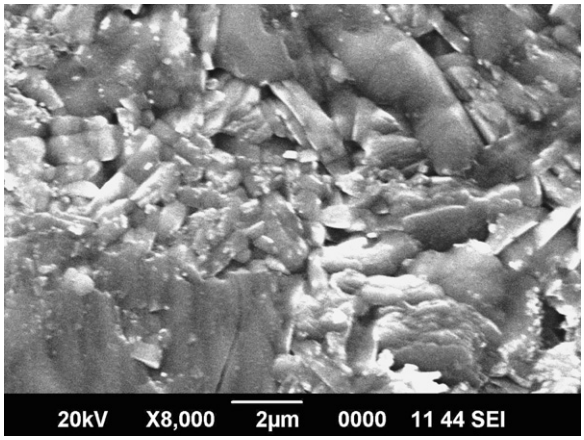

Fig. 11. SEM image of $Ba_8Mg(Nb_{3.6}Sb_{2.4})O_{24}$ ceramic.

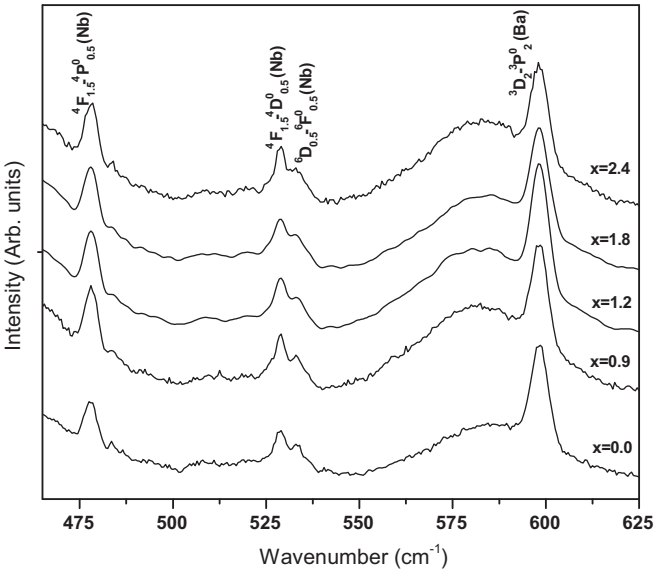

Fig. 12. PL emission spectra of $Ba_8Mg(Nb_{6-x}Sb_x)O_{24}$ ceramics.

4. Conclusions

$Ba_8Mg(Nb_{6-x}Sb_x)O_{24}$ (x = 0, 0.3, 0.6, 0.9, 1.2, 1.5, 1.8 and 2.4) ceramics are prepared through the conventional solid-state route. The materials are calcined at 1200 °C and sintered at 1375 °C. The structure of the system is analyzed by XRD, FT-IR and Raman spectroscopy. The theoretical and experimental densities are calculated. The dielectric constant (ε_r), temperature coefficient of resonant frequency (τ_f) and the unloaded quality factor (Q_u) are measured in the microwave frequency region. The τ_f values of the samples reduced considerably with the increase in the Sb content. The dielectric properties are also studied in the frequency range 50 Hz to 5 MHz. The microstructures of the sintered pellets are analyzed using SEM. The photoluminescent measurements show that the materials have intense emission lines in the wavelength region 450–650 nm. The compositions have good microwave dielectric properties and photoluminescence and hence are suitable for dielectric resonator and ceramic laser applications.

Acknowledgement

The authors are thankful to Dr. M. T. Sebastian for his help in microwave measurements. Dr. Sam Solomon acknowledges University Grants Commission (UGC) for the post-doctoral research award.

References

[1] M.T. Sebastian, Dielectric Materials for Wireless Communication, first ed., Elsevier Publications, The Netherlands, 2008.
[2] W. Wersing, Curr. Opin. Solid State Mater. Sci. 1 (1996) 715.
[3] I.M. Reaney, J. Am. Ceram. Soc. 89 (2006) 2063.
[4] K. Kakegawa, T. Wakabayashi, Y. Sasaki, J. Am. Ceram. Soc. 69 (1986) c82.
[5] D.A. Sagada, S. Nambu, J. Am. Ceram. Soc. 75 (1992) 2573.
[6] M.R. Varma, S. Biju, M.T. Sebastian, J. Eur. Ceram. Soc. 26 (2006) 1903.
[7] A. Ioachim, M.I. Toacsan, M.G. Banciu, L. Nedelcu, C.A. Dutu, H.V. Alexandru, S. Antohe, E. Andronescu, S. Jinga, P. Nita, Thin Solid Films 516 (2008) 1558.
[8] K.P. Surendran, P. Mohanan, M.T. Sebastian, J. Solid State Chem. 177 (2004) 4031.
[9] M.T. Sebastian, K.P. Surendran, J. Eur. Ceram. Soc. 26 (2006) 1791.
[10] H. Yamada, T. Okawa, T. Ogihara, Key Eng. Mater. 388 (2009) 245.
[11] I. Molodetsky, P.K. Davies, J. Eur. Ceram. Soc. 21 (2001) 2587.
[12] A.M. Abakumov, J. Solid State Chem. 125 (1996) 102.
[13] S.M. Moussa, J.B. Claridge, M.J. Rosseinsky, S. Clarke, R.M. Ibberson, T. Price, D.M. Iddles, D.C. Sinclair, Appl. Phys. Lett. 82 (2003) 4537.
[14] P.K. Davies, A. Borisevich, M. Thirumal, J. Eur. Ceram. Soc. 23 (2003) 2461.
[15] M. Thirumal, P.K. Davies, J. Am. Ceram. Soc. 88 (2005) 2126.
[16] M. Barwick, F. Azough, R. Freer, J. Eur. Ceram. Soc. 26 (2006) 1767.
[17] H. Hughes, F. Azough, R. Freer, D. Iddles, J. Eur. Ceram. Soc. 25 (2005) 2755.
[18] M. Bieringer, S.M. Moussa, L.D. Noailles, A. Burrows, C.J. Kiely, M.J. Rosseinsky, R.M. Ibberson, Chem. Mater. 15 (2003) 586.
[19] S. Kawaguchi, H. Ogawa, A. Kan, S. Ishihara, J. Eur. Ceram. Soc. 26 (2006) 2045.
[20] T.H. Gfroerer, in: R.A. Meyers (Ed.), Encyclopedia of Analytical Chemistry, John Wiley & Sons Ltd., Chichester, 2000, p. 9209.
[21] L. Jacob, H.P. Kumar, K.G. Gopchandran, J.K. Thomas, S. Solomon, J. Mater. Sci.: Mater. Electron. 18 (2007) 831.
[22] M.K. Suresh, P.R.S. Wariar, J.K. Thomas, S. Solomon, J. Mater. Sci.: Mater. Electron. (2009), doi:10 1007/s10854-009-0045-7.
[23] S. Solomon, J. Alloys Compd. 506 (2010) 243.
[24] R.D. Shannon, Acta Cryst. A32 (1976) 751.
[25] C. Vijayakumar, H. Padma Kumar, V.T. Kavitha, S. Solomon, J.K. Thomas, P.R.S. Wariar, J. Koshy, J. Alloys Compd. 475 (2009) 778.
[26] R. Ratheesh, H. Sreemoolanadhan, M.T. Sebastian, J. Solid State Chem. 131 (1997) 2.
[27] C.J. Lee, G. Pezzotti, S.H. Kang, D.J. Kim, K.S. Hong, J. Eur. Ceram. Soc. 26 (2006) 1385.
[28] R. Ratheesh, M. Wöhlecke, B. Berge, Th. Wahlbrink, H. Haeuseler, E. Rühl, R. Blachnik, P. Balan, N. Santha, M.T. Sebastian, J. Appl. Phys. 88 (2000) 2813.
[29] D. Rout, G.S. Babu, V. Subramanian, V. Sivasubramanian, Int. J. Appl. Ceram. Technol. 5 (2008) 522.
[30] H. Ogawa, H. Taketani, A. Kan, A. Fujita, G. Zouganelis, J. Eur. Ceram. Soc. 25 (2005) 2859.
[31] R. Guo, A.S. Bhalla, J. Sheen, F.W. Ainger, S. Erdei, E.S. Subbarao, J. Mater. Res. 10 (1995) 18.
[32] J.C. Maxwell, A treatise on Electricity and Magnetism, 328, Oxford University Press, Oxford, U.K., 1954 (2 Section).
[33] S.V. Pol, V.G. Pol, A. Gedanken, G.I. Spijksma, J. Grinblat, R. Kalai Selvan, V.G. Kessler, G.A. Seisenbaeva, S. Gohil, J. Phys. Chem. C 111 (2007) 2484.
[34] A.T. Raghavender, K.M. Jadhav, Bull. Mater. Sci. 32 (6) (2009) 575.
[35] S. Chopra, S. Sharma, T.C. Goel, R.G. Mendiratta, Solid State Commun. 127 (2003) 299.
[36] C.G. Koops, Phys. Rev. 83 (1951) 121.